Lithos 184–187 (2014) 62–73

Contents lists available at ScienceDirect

Lithos

journal homepage: www.elsevier.com/locate/lithos

Topaz magmatic crystallization in rhyolites of the Central Andes (Chivinar volcanic complex, NW Argentina): Constraints from texture, mineralogy and rock chemistry

Anna Gioncada [a,*], Paolo Orlandi [a], Luigina Vezzoli [b], Ricardo H. Omarini [c], Roberto Mazzuoli [a], Vanina Lopez-Azarevich [c], Ricardo Sureda [c], Miguel Azarevich [c], Valerio Acocella [d], Joel Ruch [d]

[a] Dipartimento di Scienze della Terra, Università degli Studi di Pisa, Pisa, Italy
[b] Dipartimento di Scienza e Alta Tecnologia, Università dell'Insubria, Como, Italy
[c] Facultad de Ciencias Naturales, Universidad Nacional de Salta, CEGA–CONICET Salta, Argentina
[d] Dipartimento di Scienze, Università Roma Tre, Roma, Italy

ARTICLE INFO

Article history:
Received 25 July 2013
Accepted 20 October 2013
Available online 30 October 2013

Keywords:
Topaz-bearing rhyolite
Fluorine
Magmatic volatiles
Miarolitic texture
Central Andes

ABSTRACT

Topaz-bearing rhyolite lavas were erupted as domes and cryptodomes during the early history of the Late Miocene Chivinar volcano, in Central Andes. These are the only topaz rhyolite lavas recognized in Central Andes. Textural, mineralogical and geochemical data on the Chivinar rhyolites suggest that topaz crystallized from strongly residual, fluorine-rich, peraluminous silicate melts of topazite composition before the complete solidification of the lava domes. Crystallization of the rhyolitic magma began with sodic plagioclase and alkali feldspar phenocrysts in the magma chamber, followed by groundmass quartz + alkali feldspar + minor sodic plagioclase during dome emplacement, and terminated with quartz + topaz + vapour bubbles forming small scattered miaroles. Fluorine partitioning into the fluid phase occurred only in the final stage of groundmass crystallization. The magmatic origin of topaz indicates the presence of a fluorine-rich highly differentiated magma in the early history of the Chivinar volcano and suggests the possibility of rare metals mineralizations related to the cooling and solidification of a silicic magma chamber. A late fluid circulation phase, pre-dating the andesitic phase of the Chivinar volcano, affected part of the topaz rhyolite lavas. The presence of Nb, Ta and Mn minerals as primary accessories in the rhyolites and as secondary minerals in veins suggests a connection of the fluid circulation phase with the silicic magmatic system. Although at the edge of the active volcanic arc, the Chivinar topaz rhyolites are in correspondence of the transtensive Calama–Olacapato–El Toro fault system, suggesting preferred extensional conditions for the formation of magmatic topaz in convergent settings, consistently with evidence from other known cases worldwide.

1. Introduction

Although more frequently interpreted as the product of post-magmatic vapour-phase alteration (e.g.; Taylor, 2009), topaz is also a rare primary constituent of magmatic rocks, originated by the crystallization of peraluminous and fluorine-rich silicic magmas (Agangi et al., 2010; Lukkari, 2002; Scaillet and MacDonald, 2004). The silicate melts enriched in fluorine have particular physical properties, i.e. low viscosity and density (Aiuppa et al., 2009). These enhance the efficiency of the petrogenetic processes, allowing segregation of unusually low fractions of partial melt from the source, as well as favouring crystal-melt fractionation during magma ascent. By that, fluorine (F) promotes the production and release of very small volumes of felsic magma enriched in a wide variety of incompatible elements (Keppler, 1993) and, consequently, potentially related to economically interesting ore mineralizations (e.g.; Burt et al., 1982; Xie et al., 2013).

In this paper we report the occurrence and the mineralogical, petrographic and chemical characteristics of rhyolitic lavas bearing topaz from the Late Miocene Chivinar volcano, located in Central Andes (Fig. 1; Koukharsky et al., 1991; Orlandi et al., 2011). While several high-silica, topaz-bearing rhyolitic lavas of Cenozoic age have been recognized in North America (western United States and Mexico; Christiansen et al., 1986; Huspeni et al., 1984; Sinclair, 1986; Rodríguez-Ríos et al., 2007), the Chivinar topaz rhyolites are, to date, the only occurrence in the Andes of South America.

Owing to their location at the intersection of the Andean active magmatic arc with a major NW-striking fault system (Fig. 1A) and to their peculiar mineralogy, the Chivinar rocks present a two-fold interest. First, the knowledge of the petrogenetic processes responsible for the composition of these lavas may add new elements for the interpretation of the genesis and evolution of magmas at the arc-back-arc boundary in Central Andes (Acocella et al., 2011; Matteini et al., 2002). Second,

* Corresponding author.
E-mail address: gioncada@dst.unipi.it (A. Gioncada).

0024-4937/$ – see front matter © 2013 Elsevier B.V. All rights reserved.
http://dx.doi.org/10.1016/j.lithos.2013.10.023

understanding the origin of topaz in magmatic rocks may contribute to explain mineralizations in rare, economically interesting elements (Xie et al., 2013 and references therein). For both purposes, the determination of the primary (magmatic) vs. secondary (hydrothermal) origin of topaz is crucial. This contribution presents the textural, mineralogical and geochemical constraints to the magmatic origin of topaz in the Chivinar rhyolite and proposes a model for the magmatic crystallization of topaz rhyolite.

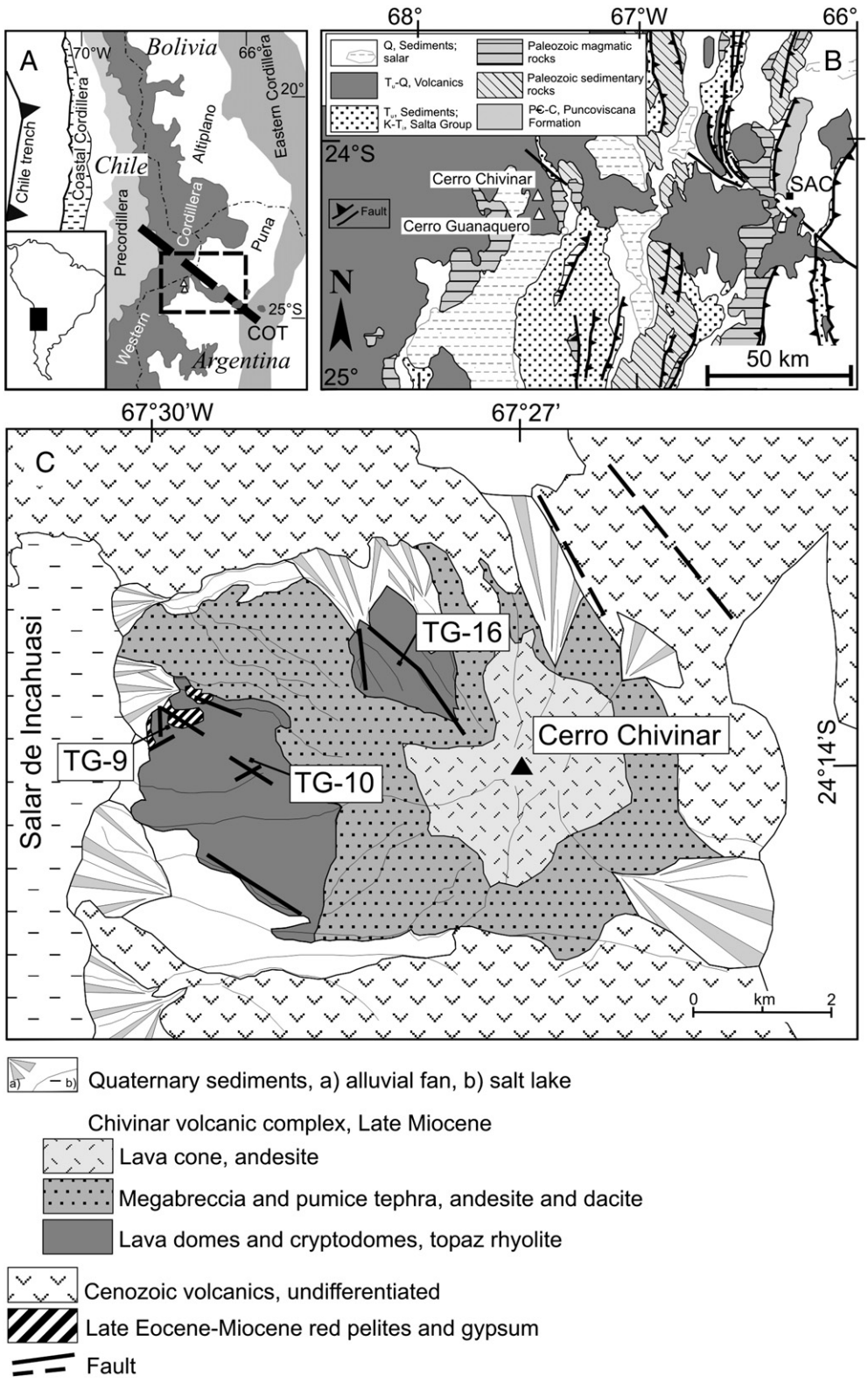

Fig. 1. Geological framework of the Chivinar volcanic complex. (A) Location of the studied area with respect of the morpho-structural units of the Central Andes. The Western Cordillera is the active magmatic arc. Miocene to Quaternary volcanism develops in the backarc along some transverse NW-trending lineaments as the Calama–Olacapato–El Toro (COT) fault system. (B) Regional geologic map of the Puna plateau showing the location of the Chivinar volcano at the boundary between the magmatic arc and backarc. SAC: San Antonio de los Cobres. (C) Geologic map of the Chivinar volcano based on our new field mapping. Location of the samples studied is shown.

2. Geological framework

Cerro Chivinar is a Miocene volcano located in the western Puna plateau of the Central Andes (24°14′S–67°27′W; 5125 m above sea level, a.s.l.), at the intersection between the N–S trending active magmatic arc (Western Cordillera) and the NW–SE trending Calama–Olacapato–El Toro (COT) transtensive fault zone (Acocella et al., 2011; Salfity, 1985) (Fig. 1A and B). The COT fault zone coincides with a well-defined volcanic belt, consisting of stratovolcanoes, lava domes and some monogenetic scoria centres and formed in the last 15 Ma. The composition of the magmas erupted along the COT volcanic belt includes calcalkaline magmas ranging from basaltic andesites to dacites and rhyolites, and shoshonitic magmas erupted at the mafic monogenetic scoria centres (Acocella et al., 2011 and references therein).

The geology of the Chivinar volcano has been never described in detail. The main geological features were formerly sketched in Koukharsky and Munizaga (1990) and Koukharsky et al. (1991), reporting the occurrence of topaz in the rhyolitic lavas of the volcano. Our new geologic field mapping shows that Chivinar is a polygenetic volcanic complex built by three superposed and distinct eruptive packages (Figs. 1C and 2A). The oldest unit is made up of a cluster of topaz rhyolite lava domes exposed on the N and W basal platform of the volcano, between 3500 and 4000 m a.s.l.. The following unit consists of radially emplaced coarse dacite breccia and pumice deposits that resulted from lava dome catastrophic destruction events. Finally, an andesite lava cone caps the volcanic edifice. A K/Ar age of 9.0 ± 0.4 Ma was determined on andesite of the Chivinar lava cone (Koukharsky and Munizaga, 1990). The substratum of the volcano is represented by continental terrigenous and evaporitic deposits of Late Eocene–Miocene age (Fig. 1B; Geste, Pozuelos and Sijes Formations; Blasco et al., 1996; Jordan and Alonso, 1987). The most active tectonic systems are WNW–ESE trending transtensive and extensional faults (Figs. 1 and 2), similarly to the ones found along the eastern continuation of the COT (Acocella et al., 2011). These systems seem also to control the preferred WNW–ESE elongation of the volcano.

The Chivinar topaz rhyolites consist of a group of coalescent lava domes that were extruded as small, endogenous lava domes and shallowly emplaced intrusive domes and plugs (Fig. 1C). The lava emplacement lacks of associated explosive products. Field evidence excludes the association of the rhyolite with one or more caldera structures. Rhyolite rests directly on or intrudes the Eocene–Miocene sedimentary substratum (Fig. 2B). Intrusive and cooling histories of individual lava bodies are locally constrained by lava textures, as marginal vitrophyres, flow-banding and breccias, at the contact with host sediments. The remnant domes range from 0.3 to 1 km in diameter and are up to 250 m high. The rhyolite dome field makes up nearly one third of the volume of the Chivinar complex.

At the end of the oldest Chivinar eruptive episode, the rhyolite lavas were intensely deformed, eroded and altered. The pervasiveness of the deformation and hydrothermal alteration contrasts with the fresh younger breccias and lavas that make up the rest of the edifice, suggesting that tectonism and fluid circulation followed by exogenous weathering occurred prior to renewed construction of the edifice.

3. Sampling and analytical methods

Three samples of the rhyolitic domes showing no macroscopic evidence of alteration were selected for the preparation of polished thin sections and for crushing and powdering. TG-9 rhyolite represents the external part of a dome near the contact with the host evaporitic rock; TG-10 and TG-16 come from the inner part of the coalescent dome cluster (Figs. 1C and 2). Also, three samples of the rhyolites were collected from outcrops showing hydrothermal alteration evidence, to evaluate the relationships between the primary and secondary mineralogy. Finally, representative samples of the Chivinar dacites and andesites capping the volcanic edifice were selected for comparing the major elements composition with the silicic lavas.

Whole-rock X-ray fluorescence (XRF) analyses of major oxides were done on fused samples with an ARL 9400 XPp instrument at the Dipartimento di Scienze della Terra, University of Pisa, Italy. Accuracy is 4–7% for concentrations <1 wt.%, 2–4% for concentrations 1–10 wt.%, 1% for concentrations >10 wt.%. Trace-element analyses and Loss on Ignition determinations were carried out on powdered rock samples at Als Laboratories, Seville, Spain.

Microanalytical data were collected on polished and carbon-coated rock sections with a Philips XL30 scanning electron microscope equipped with microanalysis EDAX (standard-less software DXi4) at Dipartimento di Scienze della Terra, University of Pisa, Italy (acceleration voltage 20 kV, beam current 5 nA, live time 100 s). The accuracy is better than 0.5% if abundance is >15 wt.%, 1% if abundance is around 5 wt.%, and better than 20% if abundance is around 0.5 wt.%.

Mineral separations were carried out to investigate the heavy mineral fraction by means of SEM–EDS with the above described facilities. XRD analysis of selected mineral grains was carried out at Dipartimento di Scienze della Terra, University of Pisa with a Gandolfi camera (114.6 mm in diameter) and CuKα radiation.

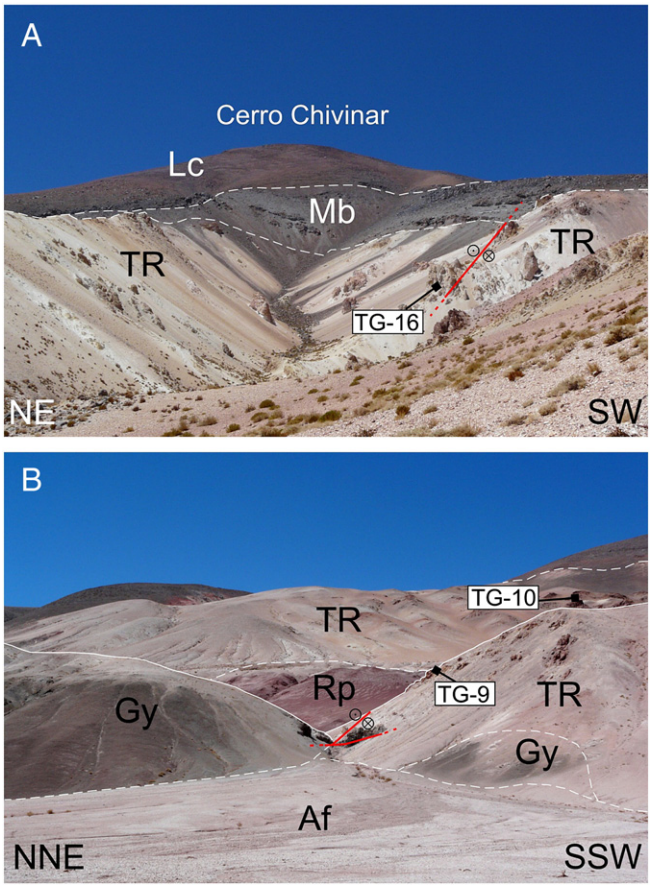

Fig. 2. Fig. 2. Field photos of volcanic features of the Cerro Chivinar volcanic complex. Location of the studied samples is also shown. (A) The northern flank of the Cerro Chivinar shows three superposed and distinct eruptive packages, from bottom: TR = topaz-bearing rhyolite lava domes; Mb = dacite megabreccia and pumice deposits; Lc = andesite lava cone. The red line is the trace of the major NW–SE striking transtensive fault (white circles indicate a sinistral kinematics). (B) The western flank of the Cerro Chivinar shows the stratigraphic and intrusive relationships between the topaz-bearing rhyolite lava domes (TR) and the Eocene–Miocene sedimentary substratum (Rp = red pelites; Gy = gypsum). Af = alluvial fan. Red lines are the traces of the major NW–SE transtensive (white circles indicate a sinistral kinematics) and NS transpressive striking faults.

4. Petrography and mineral chemistry

The Chivinar rhyolites are characterized by a very homogeneous white to creamy white colour. The hand samples show porphyritic texture, with about 10% in volume of transparent phenocrysts, 0.5 to 3 mm in size, rare coloured minerals, <1 mm in size, and very fine voids. Neither xenocrysts nor xenoliths from the andesitic magmatic system have been found in the silicic lava samples.

The phenocrysts are plagioclase, consisting of euhedral stubby oligoclase with moderate direct zoning, and sanidine, with low 2 V angle (15–20°), with elongated lath shape and lower size than plagioclase (Figs. 3 and 4A–B; Table 1). In sample TG-9, oligoclase is the only phenocryst.

The groundmass of the Chivinar rhyolites is holocrystalline and shows a fine-grained (40–100 μm), isotropic granular texture, consisting of equant subidiomorphic quartz, alkali feldspar and sodic plagioclase (Fig. 4B–C). The quartz microlites locally show rounded corners.

Trails of minute vapour-rich secondary fluid inclusions cross-cutting phenocrysts are rather common (Fig. 4A). The groundmass crystals mainly host solid inclusions of accessory minerals and minute vapour-rich inclusions of primary formation.

Voids, mainly 50–200 μm in size, are disseminated in the lavas. The void boundaries are irregular, following the boundaries of the rock crystals, which sometimes protrude into the void.

The composition of plagioclase phenocrysts is quite constant, with modest direct zoning $An_{15}Ab_{79}$–$An_{10}Ab_{85}$, and the groundmass microlites have the same composition of the phenocryst's rims. The composition of alkali feldspar covers the range of $Or_{65}Ab_{35}$–$Or_{51}Ab_{47}$ from phenocrysts to groundmass microlites (Fig. 3). The alkali feldspar crystals in the groundmass show subtle lamellae of Na-rich feldspar, 0.5–1 μm thick (Fig. 4D), developing preferentially from the rim inward.

The average volume proportions of quartz, plagioclase and alkali feldspar in the rocks are 36 ± 2, 14 ± 3 and 49 ± 2 vol.%, respectively, determined with image analysis using microphotos and backscattered electrons SEM images (ImageJ version 1.42q). Several other minerals occur in <3 vol.% to trace amounts, including topaz, magnetite, both interstitial and included in quartz, ilmenite, a F-bearing tri-octahedral mica (montdorite/fluor-phlogopite; see Table 1), calcic amphibole, zircon and xenotime-Y. Zircon and xenotime-Y are commonly included in feldspar phenocrysts (Fig. 4B). In addition, topaz, zircon and xenotime sometimes show crystallization with idiomorphic terminations in voids (Fig. 4E–F).

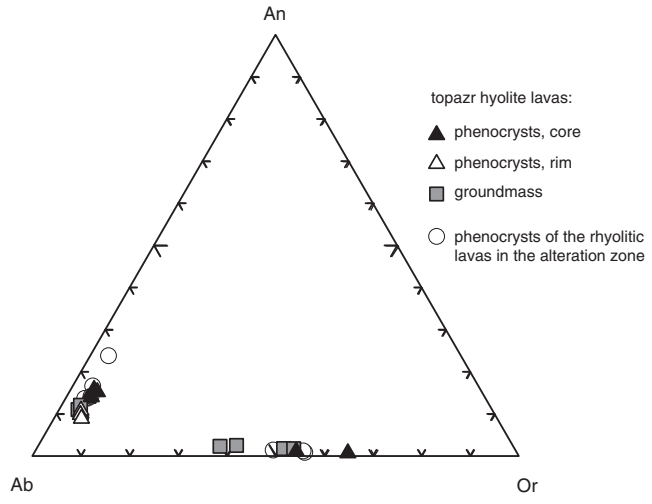

Fig. 3. Composition of feldspars of the topaz rhyolites reported in the ternary An (anorthite)–Ab (albite)–Or (orthoclase) diagram. The composition of the primary feldspars of the rhyolitic lavas in the alteration zone is also reported.

Other accessories have been identified in the heavy mineral fraction (see below). In sample TG-9, muscovite-like di-octahedral mica minerals are disseminated as clusters of fine-grained flakes in the groundmass of the lava (Table 1; Fig. 4H).

Topaz is easily encountered in the samples TG-10 and TG-16, while it is sporadic in TG-9; it occurs in the matrix in association with quartz, or forms glomeroporphyritic aggregates of acicular crystals as described in Arizona ongonites (Kortemeier and Burt, 1988). In samples TG-10 and TG-16 it concentrates in particular in correspondence of clusters of voids (e.g.; Fig. 4C–G), with both allotriomorphic and idiomorphic crystals.

The heavy mineral concentrates of the Chivinar topaz-bearing samples reveal a variety of accessory minerals in the fraction with density higher than 2.9 g/cm^3, which represent between 1 and 2 wt.% in the studied samples. The most abundant mineral phase is topaz, representing around 50% by weight of the heavy fraction (Fig. 4F), followed by a Nb-rich rutile variety. Monazite-(Ce), xenotime-(Y, REE), an Fe-bearing tourmaline variety, zircon (with Th, U and Hf) and Mn-garnet (spessartine) are present in trace amounts. All these mineralogical phases have been identified by SEM–EDS semi-quantitative chemical analyses (Table 1). The content of Nb in the presumed rutile resulted remarkably high; therefore, the identification was confirmed by an X-ray powder pattern collected with a Gandolfi camera.

In the samples from the outcrops affected by hydrothermal alteration, the rhyolitic lavas show the same primary mineralogy and texture of the unaltered samples. They are porphyritic, with millimetric plagioclase and sanidine phenocrysts in a quartz-feldspathic groundmass. The secondary minerals are both disseminated and in veinlets that stand out for their dark green to black colour (Fig. 4I–J) and include Mn-bearing silicates (Mn-bearing sodic amphibole and sodic pyroxene), Mn-bearing Fe–Ti oxides of the magnetite and ilmenite series, Mn-bearing apatite and Nb–Ta-bearing rutile (Table 2). Secondary alkali feldspar occurs in the host rock at the vein contact (Table 2). In some places, instead, alteration resulted in complete leaching of feldspars and silicification, with the resultant rock composed of relict fine-grained quartz and scattered Nb–Ta-bearing rutile and secondary silica phases.

The rocks of the Chivinar volcanic units following the rhyolitic lava domes are mainly andesitic lavas and minor pumiceous deposits. They are porphyritic, with phenocrysts of plagioclase and hornblende, minor orthopyroxene and scarce clinopyroxene, biotite and Fe-oxides in a groundmass made of the same mineral phases and a variable amount of glass. The least evolved andesite samples show abundant olivine phenocrysts with iddingsite rims.

5. Whole-rock major and trace element composition

The composition of the Chivinar topaz-bearing lavas falls in the TAS diagram in the rhyolite field, with a $Na_2O + K_2O$ around 8 wt.% (Fig. 5A) and $K_2O/Na_2O = 1$ (Table 3). The rhyolites with silica around 75–77 wt.% are peraluminous and corundum appears in their CIPW norm, while the TG-9 rhyolite with 74 wt.% SiO_2 is metaluminous. The composition of other volcanic rocks forming the Chivinar volcanic complex is remarkably different, ranging in silica from 59 to 63 wt.% (Fig. 5A): the pumice clasts in the pyroclastic breccias are dacites and the final lava flows are andesites, belonging to the high-K calcalkaline series.

A comparison of the Chivinar rhyolites with other topaz-bearing silicic rocks indicates similarly high Rb, Th, U, Pb, and Y but even higher Nb, Ta, while the LREE values are lower (e.g.; Christiansen et al., 1983, 1986, 2007; Lukkari, 2002; Rodríguez-Ríos et al., 2007) (Fig. 5B, C). The REE patterns are notably flat, with $(La/Yb)_n = 2.5$, and display a strong Eu negative anomaly, with $Eu/Eu^* = 0.11$ (Fig. 5B).

The Chivinar rhyolites have the same geochemical characteristics (P_2O_5 <0.1 wt.%, Al_2O_3 <14.5 wt.%, SiO_2 >73 wt.%) of the low-P_2O_5 subtype of topaz-granites after Taylor and Fallick (1997), and of low-P_2O_5

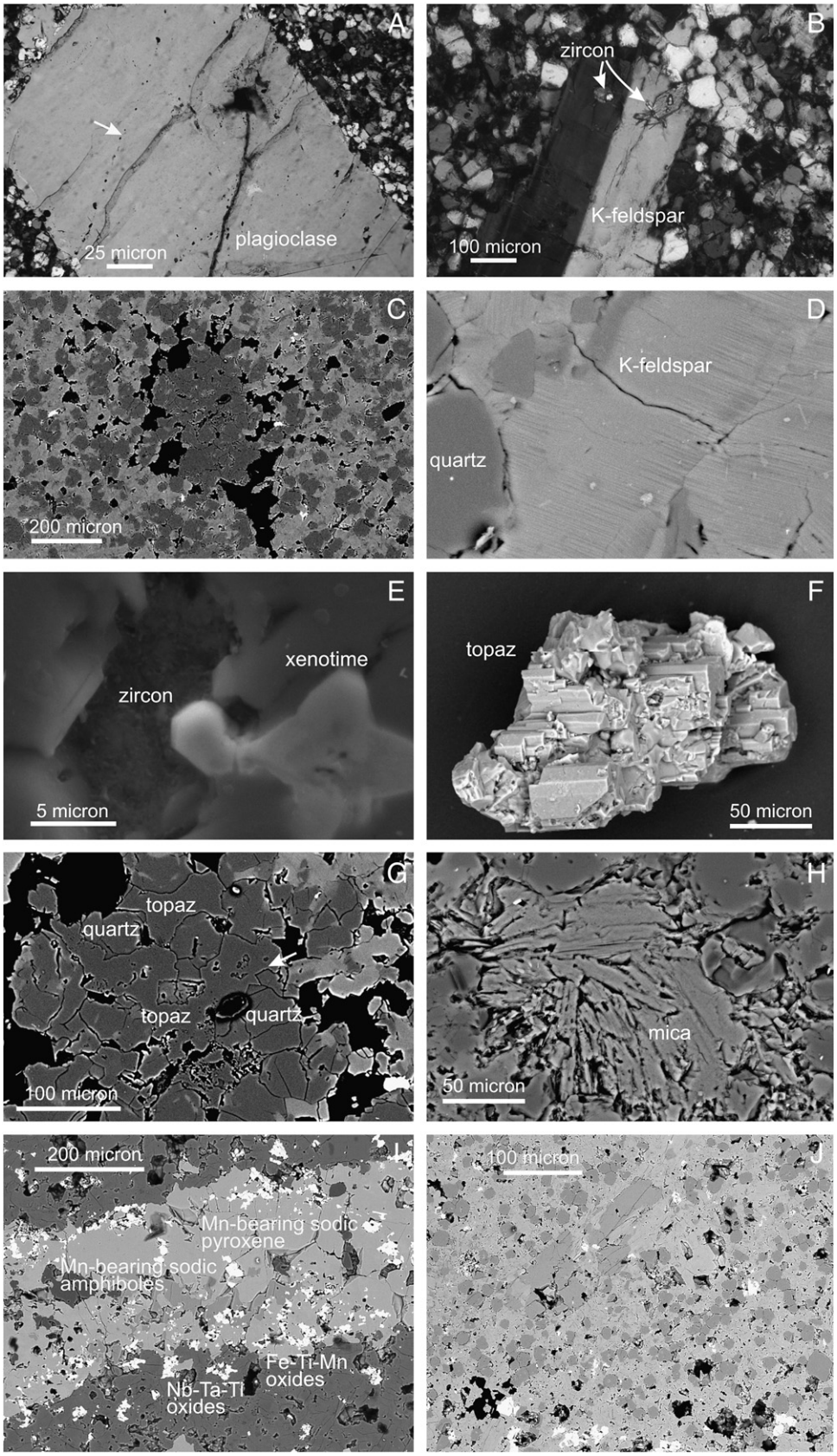

Fig. 4. Petrographic thin section photos with crossed nicols (A, B) and backscattered electrons SEM images (C…J) of Chivinar topaz rhyolite samples. A. Fluid inclusion trails in plagioclase phenocryst (arrow shows an example). B. Sanidine phenocryst and zircon, xenotime accessories in the holocrystalline, equant, quartz–feldspathic groundmass. C. Topaz concentration with voids. D. Cryptoperthitic lamellae in alkali feldspar in the topaz rhyolite, testifying the final slow cooling phase of the lava dome; note the homogeneous core, representative of a former crystallization step at higher temperature. E. Zircon in void, in epitaxis with xenotime. F. Topaz, with syntaxial growth. G. Textural relationships between topaz and quartz (arrow indicates quartz–topaz contact). Note the frequent fluid inclusions in topaz. H. Di-octahedral mica flakes in the groundmass of Chivinar rhyolites, sample TG-9. I. Detail of veinlet in Chivinar rhyolite. Secondary minerals in vein are Mn-bearing amphiboles and Nb-bearing oxide. J. Detail of the rhyolite hosting veinlet in I: note the disseminated Nb–Ta–Ti oxides, compared to the rhyolite lava in C.

Table 1
Representative EDS analyses of primary minerals in the Chivinar rhyolitic lavas.

Sample	TG-16	TG-16	TG-16	TG-16	TG-16	TG-16	TG-9	TG-16	TG-16	TG-16	TG-16	TG-16	TG-9
	pl	*pl*	*pl*	*pl*	*pl*	*pl*	*pl*	*pl*	*pl*	*Kf*	*Kf*	*Kf*	*Kf*
Wt.%	Core	Rim	Core	Rim	Core	Rim	Core	grm	grm	Core	grm	grm	grm
SiO_2	64.37	65.38	64.09	65.90	63.46	65.46	63.61	65.30	64.76	65.29	65.70	65.52	65.12
Al_2O_3	22.49	21.71	22.70	21.58	23.11	22.03	23.02	21.80	22.67	19.53	19.49	19.43	19.36
FeO	bdl	0.15	bdl	0.07	0.14	bdl	bdl	bdl	0.26	bdl	bdl	0.20	0.07
CaO	2.86	1.86	3.15	1.99	3.28	2.07	3.42	2.32	2.40	0.14	0.37	0.36	0.24
Na_2O	9.48	9.90	9.06	9.59	9.15	9.59	9.03	9.89	9.26	3.94	5.50	5.23	3.62
K_2O	0.81	1.00	1.01	0.86	0.85	0.85	0.92	0.69	0.65	11.11	8.94	9.26	11.60
An	13.63	8.87	15.18	9.77	15.73	10.13	16.40	11.03	12.04	0.68	1.76	1.73	1.16
Ab	81.77	85.45	79.02	85.20	79.41	84.92	78.35	85.07	84.08	34.78	47.47	45.39	31.80
Or	4.60	5.68	5.80	5.03	4.85	4.95	5.25	3.90	3.88	64.53	50.77	52.88	67.04

Sample	TG-16	TG-16		TG-16	TG-9	TG-9		TG-16
	Garnet	*Garnet*		*Tri-oct. mica*	*Di-oct. mica*	*Di-oct. mica*		*Topaz*
Wt.%			Wt.%				Wt.%	
SiO_2	37.15	34.9	SiO_2	41.90	51.74	51.01	SiO_2	33.55
Al_2O_3	20.92	20.86	TiO_2	0.99	0.08	0.22	Al_2O_3	49.32
FeO	15.81	16.34	Al_2O_3	20.71	31.18	31.22	F[a]	17.13
MnO	24.11	25.82	FeO	13.39	1.82	1.78		
MgO	1.54	1.36	MnO	4.06	0.12	0.11		
CaO	0.47	0.72	MgO	7.92	3.79	3.84		
			Na_2O	bdl	0.66	0.5		
$[Al^{VI}. Fe^{2+}]$	4.04	3.85	K_2O	11.04	10.61	11.32		
[Mn. Mg. Ca]	5.92	6.34						

[a] Semi-quantitative; bdl: below detection limit. Pl: plagioclase; Kf: alkali feldspar; grm: groundmass.

granites from Central Europe and Scandinavian described by Breiter (2012) and Lukkari (2002). The low P_2O_5 in the Chivinar topaz rhyolites is in agreement with the absence of apatite as accessory (all Ca contributed to plagioclase) and contributes to distinguish these silicic magmas from S-type peraluminous magmas, suggesting a derivation by partial melting of an igneous protolith rather than of a pelitic one. In the discrimination diagram suggested by Whalen et al. (1987) for granites, the Chivinar topaz rhyolites fall in the field for intraplate settings (Fig. 6). The North America topaz rhyolites show the same major element characteristics and similarly high Nb content and Nb/Y value (Fig. 6), and are explained with melting of continental crust previously intruded by mafic magmas with an intraplate signature (Christiansen et al., 2007; Rodríguez-Ríos et al., 2007).

6. Discussion

Whether topaz has a late magmatic (primary) or hydrothermal (secondary) origin has been a matter of discussion for several silicic igneous complexes. There is abundant petrographic evidence for topaz having formed as a liquidus phase in many topaz granites (Lukkari, 2002; Taylor, 1992) and, also, in sub-volcanic rhyolites (Xie et al., 2013). Indeed, the occurrence of melt inclusions in topaz has been taken as a proof of a magmatic origin for topaz hosts (Eadington and Nashar, 1978). Nevertheless, topaz is a frequent greisen mineral and in granites it has often been considered a sub-solidus replacement phase linked to autometasomatic processes, i.e. to alteration by the last water-rich fluid trapped within the rock, or to external fluids (Kleeman, 1985; Manning and Exley, 1984). Sometimes, it is developed in miarolitic cavities of granites and pegmatites as a late vapour phase (e.g.; Colombo et al., 2009; Williamson et al., 1997).

6.1. Textural and compositional evidence for a primary crystallization of topaz in the Chivinar rhyolite

The topaz crystals in the Chivinar rhyolitic lavas show different modes of occurrence. Two of these suggest igneous textural relationships: (a) in correspondence of concentration of voids, topaz forms anhedral/subhedral grains in association with quartz (Fig. 4C–G); (b) scattered in the matrix, topaz forms glomeroporphyritic elongate grains, again in association with quartz but without a noticeable concentration of voids. A third mode of occurrence (c) is within voids, where it shows idiomorphic terminations (Fig. 4F) indicating crystallization in fluid-filled cavities. Topaz is never associated to secondary minerals; indeed, the Chivinar rhyolites lack any evidence of replacement of primary minerals by secondary phases out of the alteration zone (i.e. no albite, sericite or topaz replacing plagioclase and alkali feldspar). White mica is frequently encountered in sample TG-9, but it is never found in replacement of feldspars; rather, it is interstitial in the groundmass, suggesting crystallization from the residual melt. Moreover, the miaroles in all the samples are never lined or filled by secondary phases. Thus, all topaz occurrences in the Chivinar rhyolite belong to the final phases of magmatic crystallization of the rhyolitic magma.

From the point of view of the chemical composition, the presence of magmatic topaz requires a fluorine-rich and peraluminous melt. Generally, in the final stages of differentiation, rhyolitic magmas may become volatile-rich, particularly in halogens. While chlorine tends to be characteristic of peralkaline rhyolites, fluorine (and a high F/Cl) is characteristic of peraluminous rhyolites (Scaillet and MacDonald, 2004; and references therein). Fluorine tends to remain in the silicate melt until late in the magma differentiation process, having a low $D_{fluid/melt}$ (0.15–0.04 is reported in peraluminous melts, see Baker and Alletti, 2012) and is not lost into the volatile phase until very low pressures (Aiuppa et al., 2009). Thus, the F content of the final Chivinar rhyolite melt was presumably very high, also in the presence of an exsolved aqueous phase. At this stage, the peraluminous composition of the Chivinar rhyolite and the subtraction of most Ca from melt by the former crystallization of plagioclase phenocrysts, favoured the crystallization of topaz in respect to fluorite. Therefore, the chemistry of the Chivinar rhyolite is in agreement with the interpretation of topaz as a primary, late magmatic phase.

Since topaz occurs in the groundmass, when it crystallized from the residual melt an aqueous fluid phase was already exsolved. This is demonstrated by the presence of fluid inclusions in crystals, also. The F vapour/melt partition coefficient depends on F abundance: concentrations as high as ≥7–8 wt.% F in melt will result in F preferentially partitioning into the fluid phase (Carroll and Webster, 1994; Dolejš

Table 2
Representative EDS analyses of secondary minerals in the Chivinar altered rhyolitic lavas.

a

Sample	18589	18589	18589	18589	18589	18589	18589	18589
	Primary feldspars					Secondary feldspars		
	grdm	grdm	c	r	r	Vein	Vein	Vein
SiO2	65.84	66.09	65.49	65.33	65.58	65.72	65.66	65.79
Al2O3	19.08	19.24	19.34	19.87	19.67	19.41	19.76	19.12
FeO	1.44	bdl	0.14	0.06	0.05	0.34	0.09	0.25
CaO	bdl	bdl	bdl	bdl	0.13	0.06	0.24	bdl
Na2O	5.25	4.81	4.26	4.97	4.99	4.93	5.75	4.75
K2O	8.39	9.86	10.77	9.77	9.58	9.54	8.5	10.09
	100.0	100.0	100.0	100.0	100.0	100.0	100.0	100.0
Recalculated based on 8 oxygens								
Si	2.97	2.98	2.97	2.95	2.96	2.97	2.96	2.98
Al	1.02	1.02	1.03	1.06	1.05	1.03	1.05	1.02
Fe	0.05	0.00	0.01	0.00	0.00	0.01	0.00	0.01
Ca	0.00	0.00	0.00	0.00	0.01	0.00	0.01	0.00
Na	0.46	0.42	0.37	0.44	0.44	0.43	0.50	0.42
K	0.48	0.57	0.62	0.56	0.55	0.55	0.49	0.58
An	0.00	0.00	0.00	0.00	0.63	0.29	1.16	0.00
Ab	48.75	42.58	37.55	43.60	43.91	43.86	50.11	41.71
Or	51.25	57.42	62.45	56.40	55.46	55.84	48.74	58.29

c: core; r: rim; grdm: groundmass; bdl: below detection limit.

b

Sample	18589	18589	18589	18589	18589	18589	18589	18589
	Vein	Vein	Vein	Vein	Vein	Vein	Vein	Vein
	Mn-bearing sodic amphibole	Mn-bearing sodic amphibole	Mn-bearing sodic amphibole	Mn-bearing sodic pyroxene	Mn-bearing sodic pyroxene	Mn-bearing sodic pyroxene	Mn-bearing sodic pyroxene	Mn-bearing sodic pyroxene
SiO_2 (wt.%)	58.96	58.08	58.63	53.93	53.45	55.28	54.31	54.34
TiO_2	bdl	bdl	bdl	bdl	bdl	bdl	bdl	bdl
Al_2O_3	0.91	0.42	0.61	0.28	0.25	0.83	0.75	0.87
FeO	19.29	21.26	21.26	29.07	27.3	29.04	26.74	28.06
MnO	4.82	5.97	5.55	4.14	6.53	2.8	5.27	4.21
MgO	6.36	4.52	4.45	0.2	0.97	0.38	0.77	0.68
CaO	0.26	0.56	0.63	3.18	4.35	0.56	3.75	2.03
K_2O	8.45	8.46	8.16	9.2	7.15	11.11	8.42	9.81
Na_2O	0.96	0.72	0.71	bdl	bdl	bdl	bdl	bdl
Total	100.01	100	100	99.99	100	100.01	100	100.00
	Cations recalculated on the basis of 23 oxygens			Cations recalculated on the basis of 6 oxygens				
Si	8.54	8.56	8.62	2.08	2.09	2.09	2.10	2.08
Al vi	0.15	0.07	0.11	0.01	0.01	0.04	0.03	0.04
Fe3+	0.13	0.06	0.01	0.51	0.34	0.59	0.40	0.53
Fe2+	2.21	2.56	2.61	0.43	0.55	0.33	0.46	0.36
Mn	0.59	0.75	0.69	0.14	0.22	0.09	0.17	0.14
Mg	1.37	0.99	0.97	0.01	0.06	0.02	0.04	0.04
Ca	0.04	0.09	0.10	0.13	0.18	0.02	0.16	0.08
Na	2.37	2.42	2.32	0.69	0.54	0.82	0.63	0.73
K	0.18	0.13	0.13	0.00	0.00	0.00	0.00	0.00

bdl: below detection limit

c

Sample	18589	18589	18589	18589	18589	18601	18601	18601
	Fe–Mn–Ti oxide	Fe–Mn–Ti oxide	Mn-bearing phillosilicate	Mn-bearing phillosilicate	Mn-apatite	Nb–Ta-bearing rutile	Nb–Ta-bearing rutile	Nb–Ta-bearing rutile
SiO_2 (wt.%)			40.83	41.92				
TiO_2	2.98	6.86	2.48	1.96		61.71	56.96	55.82
Al_2O_3	3.23	bdl	18.67	20.25				
FeO	82.39	83.54	11.08	9.62		15.53	17.08	14.57
MnO	11.02	8.18	5.68	5.36	7.21			
MgO	0.38	bdl	9.76	9.76				
CaO					59.07			
K_2O			10.36	10.34				
Na_2O			0.49	0.6				
P_2O_5					33.73			
ZnO	bdl	1.41	0.66	0.2				
Nb_2O_5						18.72	23.73	23.77
Ta_2O_5						4.05	2.23	4.74
Total	100.00	99.99	100.01	100.01	100.01	100.01	100.00	98.90

bdl: below detection limit.

and Baker, 2007; Webster, 1990). Such high concentrations are not common in nature, but could have been achieved in the very residual melt of the Chivinar rhyolite, allowing F escape into the vapour phase. This explains how crystallization of topaz could continue into the fluid-filled bubbles (Fig. 4F).

6.2. Crystallization history of the Chivinar topaz rhyolites

The composition of the Chivinar topaz rhyolite rocks, with very low Sr and Ba and high Rb and Nb, indicates that the melt was highly differentiated. The low phenocryst content of the Chivinar rhyolitic lavas suggests a low liquidus temperature, due to the presumably high F content of the silicic melt. The presence of two feldspars in equilibrium indicates subsolvus crystallization, in agreement with high P-fluid (Fig. 7). The magmatic garnet with >20 wt.% MnO indicates a relatively

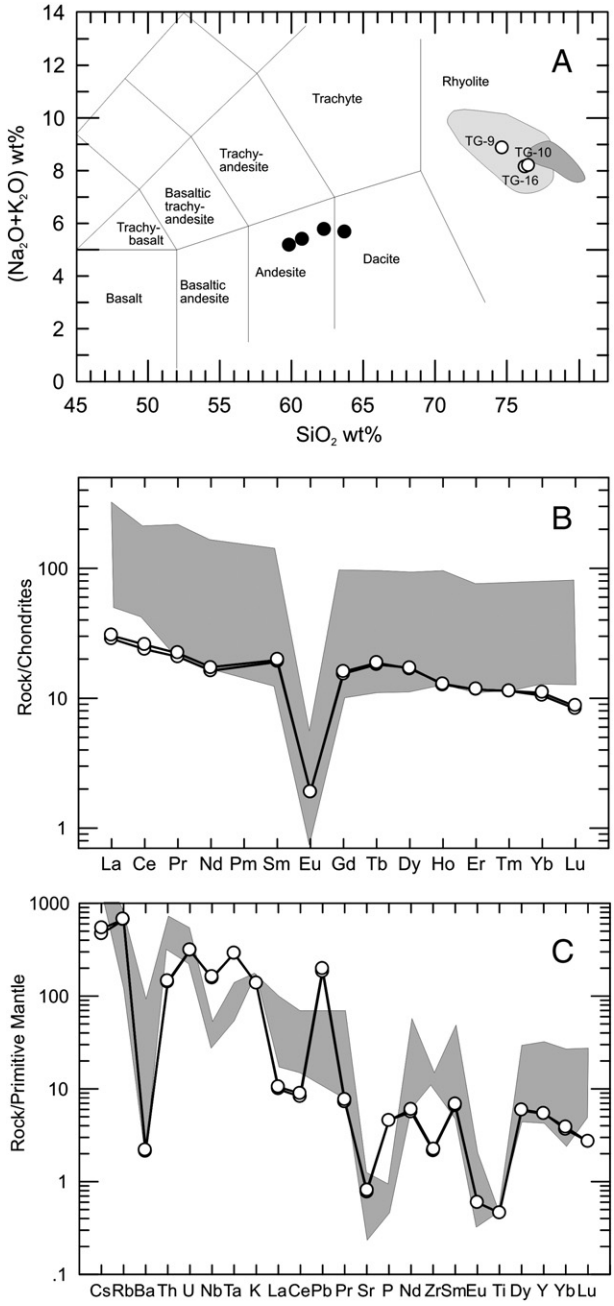

Fig. 5. A. Composition of the Chivinar rhyolites (open circles) reported in the TAS diagram (total alkali vs. silica, le Bas et al., 1986) and compared with the fields for topaz rhyolites from Christiansen et al. (2007) (light grey) and from Rodríguez-Ríos et al. (2007) (dark grey); the dashed line divides alkaline and subalkaline rocks after Irvine and Baragar (1971). The Chivinar andesitic rocks are also reported as black dots. B. Rare Earth Element patterns of the Chivinar topaz rhyolites normalized to chondrite after Sun and McDonough (1989). Symbols and fields as in Fig. 5A. C. Multielement spider diagrams of the Chivinar topaz rhyolites normalized to Primitive Mantle after Sun and McDonough (1989). Symbols and fields as in Fig. 5A.

Table 3
A. Whole rock major element composition and CIPW norm of the analyzed Chivinar rocks. ASI: Alumina Saturation Index, molecular $[Al_2O_3] / [CaO] - 1.67 * [P_2O_5] + [Na_2O] + [K_2O]$. B Trace element composition of the Chivinar topaz rhyolites.

a

Sample	TG 17	TG 11	TG 18	TG 14	TG9	TG16	TG10
SiO_2 (wt.%)	59.85	60.74	62.14	63.78	74.68	76.43	76.49
TiO_2	0.96	0.88	0.73	0.75	0.06	0.05	0.05
Al_2O_3	16.98	16.92	16.84	16.20	14.16	14.41	14.42
$Fe_2O_{3\ tot.}$	7.06	6.80	6.08	5.55	0.39	0.23	0.20
MnO	0.13	0.12	0.10	0.10	0.01	0.02	0.02
MgO	3.03	2.81	2.37	2.48	0.30	0.05	0.08
CaO	6.50	6.11	5.69	5.19	1.42	0.54	0.50
Na_2O	2.96	3.05	3.32	2.89	4.25	4.08	4.00
K_2O	2.19	2.26	2.42	2.79	4.64	4.10	4.15
P_2O_5	0.33	0.31	0.31	0.28	0.08	0.09	0.09
LOI	0.78	1.34	1.55	2.50	1.65	0.87	0.93
ASI	0.91	0.93	0.93	0.96	0.98	1.20	1.21
q	14.1	15.15	16.21	20.13	28.9	36.0	36.4
pl	52.0	51.93	52.29	47.65	41.8	36.6	35.7
or	13.0	13.41	14.36	16.55	27.5	24.2	24.5
c	0.0	0.0	0.0	0.0	0.0	2.5	2.7
di	3.0	2.10	1.93	0.75	0.5	0.0	0.0
hy	13.9	13.51	11.76	11.23	0.8	0.3	0.3
il	1.8	1.69	1.39	1.42	0.1	0.1	0.1
mt	1.6	1.49	1.33	1.61	0.2	0.1	0.1
ap	0.8	0.72	0.72	0.65	0.2	0.2	0.2

$Fe_2O_{3\ tot.}$: all Fe recalculated as Fe_2O_3

b

Sample	TG10	TG16
Ba (ppm)	15.3	14.7
Co	<0.5	0.6
Cr	10	<10
Cs	3.71	4.16
Cu	<5	9
Ga	34.5	33.3
Hf	2.1	2.2
Mo	<2	<2
Nb	113	111
Ni	<5	<5
Pb	13	14
Rb	419	426
Sn	2	1
Sr	17.1	16.2
Ta	11.7	11.8
Th	11.8	12.25
Tl	1.7	1.7
U	6.47	6.63
V	5	<5
W	3	3
Y	24.9	24.5
Zn	23	27
La	6.8	7.2
Ce	14.6	15.8
Pr	1.98	2.11
Nd	7.6	8.1
Sm	2.91	3.01
Eu	0.11	0.11
Gd	3.18	3.29
Tb	0.68	0.7
Dy	4.36	4.3
Ho	0.72	0.73
Er	1.93	1.93
Tm	0.29	0.29
Yb	1.78	1.87
Lu	0.21	0.22
(La/Yb)n	2.46	2.48
Eu*/Eu	0.11	0.11

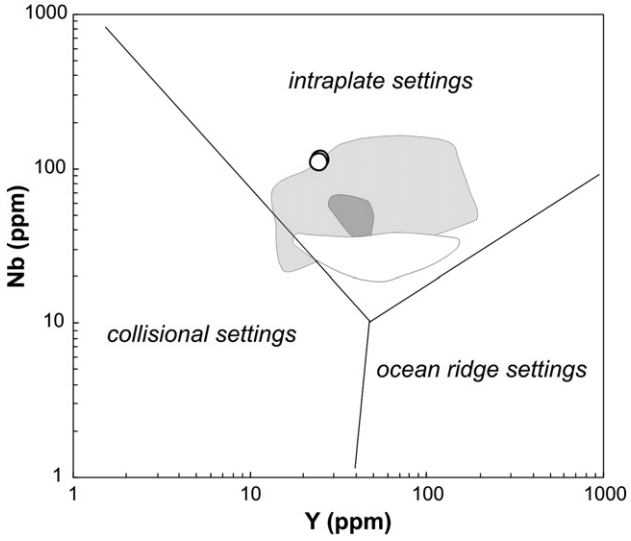

Fig. 6. Chivinar topaz rhyolites plotted in the discrimination diagram for intraplate setting after Whalen et al. (1987). Open circles are Chivinar topaz rhyolites from this work (the two samples nearly coincide); light grey field is topaz rhyolites from Christiansen et al. (2007), white field is from Rodríguez-Ríos et al. (2007), dark grey field is from Xie et al. (2013).

low crystallization pressure, <300 MPa, according to experimental and geological reconstructions in peraluminous plutons (Miller and Stoddard, 1981 and reference therein). Therefore, the storage pressure of the rhyolitic magma can be assessed at 300–400 MPa.

The crystallization temperature in the magma chamber, estimated from the phenocrysts – oligoclase and sanidine – composition, is 720–730 °C for 4 wt.% H_2O, according to the geothermometer of Putirka (2008) for a pressure of 300–400 MPa. As a comparison, 775 + 40 °C to 800 °C was calculated for Taylor Creek rhyolite, based on two feldspar equilibria and the Fe-oxides geothermometer (Duffield and Brey, 1990). The same authors estimated 700 °C to 800 °C for crystals in miarolitic cavities of Taylor Creek lava.

Quartz, sanidine and plagioclase form the groundmass crystallizing assemblage, whose nucleation was in response to magma ascent,

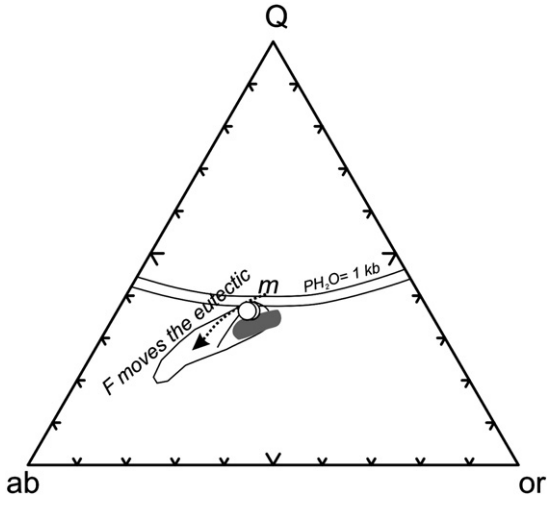

Fig. 7. The "granite" system (Qz–Ab–Or) with the composition of Chivinar topaz rhyolite rocks (open circles). The solid line indicates the quartz–feldspar cotectic and the minimum melt composition at 1 kbar, H_2O-saturated conditions (Tuttle and Bowen, 1958). The arrow shows the eutectic variation for F added to the haplogranite composition (Johannes and Holtz, 1996; and references therein). Grey field is topaz rhyolites from Christiansen et al. (2007) and white field is topaz granites from Taylor and Fallick (1997).

decompression and fluid exsolution. The size, shape and mutual relationships of the groundmass crystals, lacking the skeletal microlites indicative of high undercooling, suggest a moderate nucleation rate, as well as moderate growth rate in response to a rather slow cooling of the interior of the domes. Exsolution of an aqueous fluid, evidence of which remains in the abundant primary fluid inclusions in the late groundmass crystals (particularly in topaz) and in the trails of secondary fluid inclusions in the phenocrysts (Fig. 4A), began early during magma ascent, but was important at the late stage of groundmass crystallization. The absence of glass and of devitrification textures is in agreement with the low viscosity of the final F-rich melt, allowing element diffusion and complete groundmass crystallization during the final stages of cooling of the lava domes. The isotropic texture of the rocks indicates that crystallization took place without flowing of magma, that is after the dome emplacement.

During the slow cooling above the solidus, crystallization of the groundmass crystals (quartz, sanidine, sodic plagioclase) forced the melt composition to a very residual chemistry. The F-rich and low-viscosity interstitial melt could migrate through the microlite framework (Fig. 8), in a similar way to the gas filter-pressing process forming segregation vesicles in basaltic dykes (Sanders, 1986). This mechanism permitted the formation of the quartz + topaz + vapour bubbles concentrations, similar to the miaroles that form in felsic fine-grained intrusions crystallizing at shallow crustal levels (Fig. 8). This was because the composition of the local residual magma attained high fluorine content, resulting in moving the eutectic composition and enlarging the quartz field (Fig. 7). The residual melt at this point was probably of topazite, rather than ongonite, composition (i.e.; Kortemeier and Burt, 1988), and the fluorine content was high enough to allow F partitioning into the vapour phase and crystallization of vapour-phase topaz (Fig. 8).

The fact that the miaroles have irregular shapes, controlled by the crystals already present in the groundmass, is in agreement with their formation during a late stage release of volatiles (Vernon, 2004; Agangi et al., 2010). Besides topaz, quartz and sporadic other minerals concluded their crystallization in the fluid-filled vesicles by precipitation from the vapour phase (Candela and Blevin, 1995) (Fig. 8).

The rounded shape shown by quartz crystals in the groundmass may be due to the high volatile content of the final interstitial melt, inhibiting crystallization. Alternatively, taking into account that quartz shows resorption while feldspars do not, and that the field of stability of quartz was expanded at the expenses of feldspars by the presence of fluorine, we propose that the crystallization of topaz, decreasing fluorine in melt, may have resulted in quartz instability causing the rounded corners. Resorption of early quartz crystals in silicic systems may be caused by adiabatic decompression, also, as proposed in several recent studies (e.g. Agangi et al., 2011), but this mechanism is not suitable to explain the texture of the Chivinar rhyolites. In the Chivinar domes, rounding affects groundmass quartz microlites in the inner dome portion, therefore it occurred after dome emplacement; decompression of the partially molten dome interior after dome emplacement, possibly provoked by carapace brecciation episodes, would result in rapid microlite nucleation and growth in the residual melt, originating a texture completely different from that observed.

Cooling of the dome interior continued slowly below the solidus. The Na-rich lamellae in alkali feldspar crystals could represent exsolution lamellae due to feldspar unmixing, indicating that cooling below the solidus was sufficiently slow to allow cryptoperthite development (Fig. 4G). On the other hand, it cannot be excluded that the Na-rich lamellae indicate incipient albitization of sanidine in the presence of a Na-bearing fluid. In this hypothesis, albitization would represent a late, autometasomatic process in the interior of the dome. The discrimination between the two processes is complicated by the fact that albitization develops along the same planes of perthitic textures (Norberg et al., 2011). However, even if any albitization may have occurred, it must have been an incipient process without noticeable consequences on the rock composition.

6.3. Rare metals minerals

Accessory minerals in the Chivinar rhyolites account for their high content in Nb and Ta, and this is in agreement with the chemistry of the lavas. For instance, Nb-bearing rutile is one of the main accessories found in the heavy mineral fraction, and the partition coefficients DNb and DTa between rutile and melt for peraluminous magmas with ASI = 1.22, the same of the Chivinar rhyolite, are reported to be close to 4900 and 1900, respectively (Linnen and Keppler, 1997). The accessories are sometimes found inside phenocrysts (Fig. 4B) but they are often interstitial in the groundmass or even in correspondence of the vesicles. This indicates that they crystallized also from the final residual melt + vapour phase. This behaviour, already reported in volatile-rich silicic magmas (Agangi et al., 2010), supports a role of F-rich fluids in transporting immobile elements such as Nb and Ta.

The data collected so far indicate the existence, in Late Miocene, of a F-H_2O-rich and rare metal-rich magma chamber feeding the silicic Chivinar volcanic phase. This suggests that rare metal mineralizations formed in the Chivinar region (René and Škoda, 2011). The extent of the mineralization depends, besides the extent of the silicic magma system after the rhyolitic lava effusion, on the timing and extent of F partitioning in the fluid phase and of Nb and Ta entering accessories. The secondary mineralogy present in the Chivinar rocks, dominated by Nb–Ta–Mn oxides and silicates and devoid of chalcophile elements, and the fact that alteration affects only the rhyolitic rocks and not the younger andesite sequence, suggests a genetic link of the alteration mineralogy with the topaz rhyolite magmatic system, rather than with an andesitic one.

6.4. Geodynamic setting

In addition to the Central Andes, rhyolitic lavas with magmatic topaz have been previously found in the western United States and Mexico, in the Basin and Range Province (Burt et al., 1982; Christiansen et al., 1983, 1986, 2007), and in the Nanling Range, in southern China (Xie et al., 2013). A common feature of these provinces is the presence of lithospheric extension in an intraplate setting, with crust–mantle interaction having an important role in the generation of the magmas. Magmatism in these provinces consisted of the intrusion of hot mafic magmas at the base and within the crust, providing a heat source for partial melting. Very similar tectono-magmatic conditions are found also for the topaz rhyolites of Chivinar, in the Central Andes. Even though Chivinar lies at the edge of the N–S trending volcanic arc of the Central Andes, its main structures are the WNW–ESE transtensive faults associated with the transverse COT structure. This suggests that, from a structural point of view, rhyolitic volcanism of Chivinar may be mostly related to the back-arc transtensive conditions of COT (Acocella et al., 2011), rather than to the arc structures. In fact, even though the overall tectonic setting of the Central Andes is contractional, transtensive or extensional conditions are found along the NW–SE trending fault zones in the back-arc (e.g. Riller et al., 2001). Among these is the transtensive COT, possibly carrying most of the extension in the Central Andes (Acocella et al., 2011). In this context, the compositional features of the Chivinar topaz rhyolites, in particular the high Nb–Ta and low Y/Nb (Fig. 6), could indicate partial melting of a continental crust previously intruded by mafic igneous bodies in an extensional regime, similarly to the North America topaz rhyolites (Christiansen et al., 2007). Therefore, despite

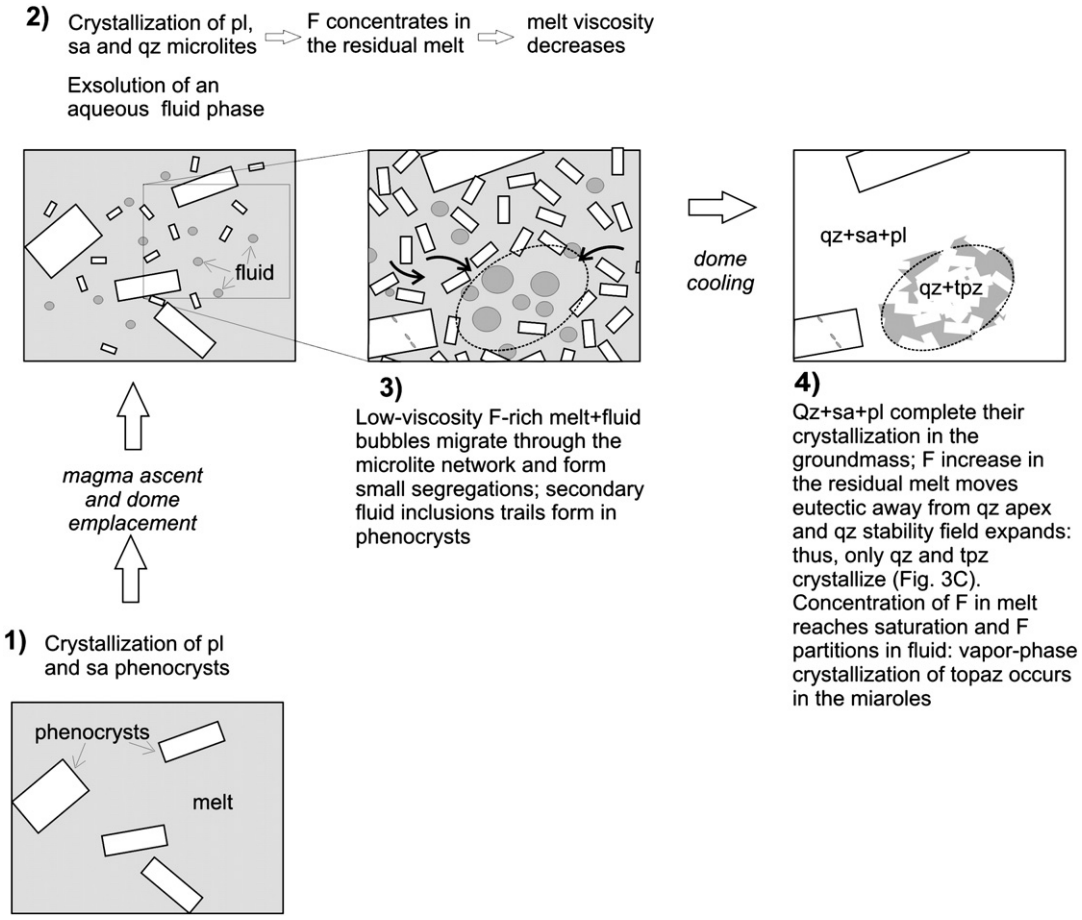

Fig. 8. Conceptual model of formation of the topaz + quartz + voids association in the Chivinar rhyolite.

the overall contractional or strike-slip setting of the arc, it is interesting to underline a connection between the transtensive/extensional features of the COT and intraplate extensional settings elsewhere. These similarities highlight preferred conditions for the formation of magmatic topaz.

7. Conclusions

The late magmatic origin of topaz in the Chivinar rhyolite lavas is supported by its igneous textural relationships with magmatic crystals and is in accordance with the peraluminous composition of the rhyolites. In addition, the topaz lacks any evidence of relationships with post-emplacement hydrothermal alteration. Textural evidence indicates that the phenocryst-poor lava of the domes interior underwent very slow cooling, and final crystallization took place in a large temperature interval. During the crystallization of the quartz–feldspathic groundmass, we propose that the F-rich, low-viscosity residual melt migrated in the crystal network and was concentrated, forming miaroles in which an assemblage topaz + quartz + vapour bubbles formed. In this final stage of groundmass crystallization, the F content in melt was so high that F could escape into the vapour phase, allowing also the final crystallization of topaz in the fluid-filled vesicles.

Given the magmatic origin of topaz, the topaz-bearing mineral assemblage in the Chivinar rhyolites suggests the existence of F-rich and rare metals-rich Late Miocene magma chambers. In addition, the alteration dominated by Nb–Ta–Mn oxides and silicates, affecting localized areas of the rhyolitic domes and pre-dating the following andesitic phase of the Chivinar volcano, suggests a genetic link with the topaz rhyolite magmatic system. This raises the possibility of the existence of veins or replacement deposits of rare metals, as well as of rare metals pegmatite bodies, in the Chivinar area.

The extensional regime due to the presence of the transtensive COT structure suggests a correspondence with topaz rhyolites in North America and China, sharing similar geochemical features unrelated to subduction, and, thus highlights preferred conditions for the formation of magmatic topaz in overall intraplate settings.

Acknowledgements

The authors thank two anonymous reviewers for their comments and suggestions. This work has been carried out in the framework of the scientific convention between Pisa (Italy) and Salta (Argentina) Universities. The research was supported by the FONCYT-AGENCIA, (PICT Nº 0745 project), Salta University Research Council (CIUNSA-Project Nº 1861) and University of Pisa funds.

References

Acocella, V., Gioncada, A., Omarini, R., Riller, U., Mazzuoli, R., Vezzoli, L., 2011. Tectonomagmatic characteristics of the back-arc portion of the Calama–Olacapato–El Toro Fault Zone, Central Andes. Tectonics 30, TC3005. http://dx.doi.org/10.1029/2010TC002854.

Agangi, A., Kamenetsky, V., McPhie, J., 2010. The role of fluorine in the concentration and transport of lithophile trace elements in felsic magmas: insights from the Gawler Range Volcanics, South Australia. Chemical Geology 273, 314–325.

Agangi, A., McPhie, J., Kamenetsky, V.S., 2011. Magma chamber dynamics in a silicic LIP revealed by quartz: the Mesoproterozoic Gawler Range Volcanics. Lithos 126, 68–83.

Aiuppa, A., Baker, D.R., Webster, J.D., 2009. Halogens in volcanic systems. Chemical Geology 263, 1–18.

Baker, D.R., Alletti, M., 2012. Fluid saturation and volatile partitioning between melts and hydrous fluids in crustal magmatic systems: the contribution of experimental measurements and solubility models. Earth-Science Reviews 114, 298–324. http://dx.doi.org/10.1016/j.earscirev.2012.06.005.

Blasco, G., Zappettini, E.O., Hongn, F., 1996. Hoja geológica 2566-1, San Antonio de los Cobres, Programa Nac. de Carteas Geol. de la Repub. Argentina, Dirección. Nacional del Servicio Geológico, Buenos Aires, Argentina.

Breiter, K., 2012. Nearly contemporaneous evolution of the A- and S-type fractionated granites in the Krušné hory/Erzgebirge Mts., Central Europe. Lithos 151, 105–151.

Burt, D.M., Sheridan, M.F., Bikun, J.V., Christiansen, E.H., 1982. Topaz rhyolites: distribution, origin, and significance for exploration. Economic Geology 77, 1818–1836.

Candela, P.A., Blevin, P.L., 1995. Do some miarolitic granites preserve evidence of magmatic volatile phase permeability? Economic Geology 90, 2310–2316.

Carroll, M.R., Webster, J.D., 1994. Solubilities of sulfur, noble gases, nitrogen, chlorine, and fluorine in magmas. Reviews in Mineralogy and Geochemistry 30, 231–279.

Christiansen, E.H., Burt, D.M., Sheridan, M.F., Wilson, R.T., 1983. The petrogenesis of topaz rhyolites from western United States. Contributions to Mineralogy and Petrology 83, 16–30.

Christiansen, E.H., Burt, D.M., Sheridan, M.F., 1986. The geology of topaz rhyolites from the western United States. Geological Society of America, Special Paper 205, 82.

Christiansen, E.H., Haapala, I., Hart, G.L., 2007. Are Cenozoic topaz rhyolites the erupted equivalents of Proterozoic rapakivi granites? Examples from the western United States and Finland. Lithos 97, 219–246.

Colombo, F., Lira, R., Pannunzio Miner, E.V., 2009. Mineralogical characterization of topaz from miarolitic pegmatites and W-bearing greisen in the A-type El Portezuelo Granite, Papachacra (Catamarca Province). Revista Asociación Geológica Argentina 64 (2), 194–200.

Dolejš, D., Baker, D.R., 2007. Liquidus equilibria in the system K_2O–Na_2O–Al_2O_3–SiO_2–F_2O1–H2O to 100 MPa: II. Differentiation paths of fluorosilicic magmas in hydrous systems. Journal of Petrology 48 (4), 807–828.

Duffield, W.A., Brey, E.A., 1990. Temperature, size, and depth of the magma reservoir for the Taylor Creek Rhyolite, New Mexico. American Mineralogist 75, 1059–1070.

Eadington, P.J., Nashar, B., 1978. Evidence for the magmatic origin of quartz–topaz rocks from the New England Batholith, Australia. Contribution Mineralogy and Petrology 67, 433–438.

Huspeni, J.R., Kesler, S.E., Ruiz, J., Tuta, Z., Sutter, J.F., Jones, L.M., 1984. Petrology and geochemistry of rhyolites associated with tin mineralization in northern Mexico. Economic Geology 79, 87–105.

Irvine, T.N., Baragar, W.R.A., 1971. A guide to chemical classification of the common rocks. Canadian Journal of Earth Science 8, 523–548.

Johannes, W., Holtz, F., 1996. Petrogenesis and Experimental Petrology of Granitic Rocks. Springer-Verlag, Berlin (335 pp.).

Jordan, T.E., Alonso, R.N., 1987. Cenozoic stratigraphy and basin tectonics of the Andes Mountains 20°–28° South Latitude. The American Association of Petroleoum Geologists Bulletin 71, 49–64.

Keppler, H., 1993. Influence of fluorine on the enrichment of high field strength trace elements in granitic rocks. Contribution to Mineralogy and Petrology 114, 479–488.

Kleeman, J.D., 1985. Origin of Disseminated Wolframite-Bearing Quartz–Topaz Rock at Torrington, New South Wales, Australia. High-Heat Production (HHP) Granites, Hydrothermal Circulation and Ore Genesis.Institution of Mining and Metallurgy, London 197–201.

Kortemeier, W.T., Burt, D.M., 1988. Ongonite and topazite dikes in the Flying W ranch area, Tonto basin, Arizona. American Mineralogist 73, 507–523.

Koukharsky, M., Munizaga, F., 1990. Los volcanes Guanaquero, Chivinar, Tul Tul, Del Medio y Pocitos, provincia de Salta, Argentina. Litología y edades K/Ar. XI Congreso Geologico Argentino, San Juan. Actas, 1, pp. 64–67.

Koukharsky, M., Pereyra, F., Etcheverria, M., Lanes, S., 1991. La riolita con topacio del cerro Chivinar, Departamento Los Andes, Provincia de Salta. Revista Asociacion Geologica Argentina 46, 349–351.

Le Bas, M.J., Le Maitre, R.W., Streckeisen, A., Zanettin, B., IUGS Subcommission on the Systematics of Igneous Rocks, 1986. A chemical classification of volcanic rocks based on the total alkali-silica diagram. Journal of Petrology 27, 745–750.

Linnen, R.L., Keppler, H., 1997. Columbite solubility in granitic melts: consequences for the enrichment and fractionation of Nb and Ta in the Earth's crust. Contributions to Mineralogy and Petrology 128, 213–227.

Lukkari, S., 2002. Petrography and geochemistry of the topaz-bearing granite stocks in Artjärvi and Sääskjärvi, western margin of the Wiborg Rapakivi granite batholith. Bulletin Of The Geological Society Of Finland 74 (1–2), 115–132.

Manning, D.A.C., Exley, C.S., 1984. The origins of late-stage rocks in the St Austell granite—a re-interpretation. Journal of the Geological Society of London 141, 581–591.

Matteini, M., Mazzuoli, R., Omarini, R., Cas, R., Maas, R., 2002. The geochemical variations of the upper cenozoic volcanism along the Calama–Olacapato–El Toro transversal fault system in central Andes (~24°S): petrogenetic and geodynamic implications. Tectonophysics 345, 211–227.

Miller, C.F., Stoddard, E.F., 1981. The role of manganese in the paragenesis of magmatic garnet: an example from the old Woman-Piute range, California. Journal of Geology 89, 233–246.

Norberg, N., Neusser, G., Wirth, R., Harlow, D., 2011. Microstructural evolution during experimental albitization of K-rich alkali feldspar. Contribution to Mineralogy and Petrology 162, 531–546.

Orlandi, P., Gioncada, A., Vezzoli, L., Omarini, R., Mazzuoli, R., Lopez-Azarevich, V., Sureda, R., Azarevich, M., Bianchi, D., Acocella, V., Rusch, J., Guillou, H., Nonnotte, P., 2011. The topaz-bearing rhyolite lavas from Chivinar volcanic complex (24°17′38″S–67°25′28″W, Central Andes, NW Argentina). 1er Simposio sobre petrología ígnea y metalogénesis asociada. San Miguel de Tucumán, November 16-18, 2011.

Putirka, K., 2008. Thermometers and Barometers for Volcanic Systems. In: Putirka, K., Tepley, F. (Eds.), Minerals, Inclusions and Volcanic Processes, Reviews in Mineralogy and Geochemistry. Mineralogical Soc. Am., 69, pp. 61–120.

René, M., Škoda, R., 2011. Nb–Ta–Ti oxides fractionation in rare-metal granites: Krásno-Horní Slavkov ore district, Czech Republic. Mineralogy and Petrology 103, 37–48. http://dx.doi.org/10.1007/s00710-011-0152-z.

Riller, U., Petrinovic, I., Ramelow, J., Strecker, M., Oncken, O., 2001. Late Cenozoic tectonism, collapse calderas and plateau formation in the Central Andes. Earth Planetary Science Letters 188, 299–311.

Rodríguez-Ríos, R., Aguillón-Robles, A., Leroy, J.L., 2007. Evolución petrológica y geoquímica de un complejo de domos topacíferos en el Campo Volcánico de San Luis Potosí (México). Revista Mexicana de Ciencias Geológicas 24 (3), 328–343.

Salfity, J.A., 1985. Lineamentos transversales al rumbo andino en el noroeste argentino. Actas IV Congreso Geológico Chileno, Antofagasta, Chile 2, 119–137.
Sanders, I.S., 1986. Gas filter-pressing origin for segregation vesicles in dykes. Geological Magazine 123, 67–72.
Scaillet, B., Macdonald, R., 2004. Fluorite stability in silicic magmas. Contributions to Mineralogy and Petrology 147, 319–329.
Sinclair, W.D., 1986. Early tertiary topaz rhyolites and associated mineral deposits in the northern Canadian Cordillera; products of anorogenic magmatism. Program with abstracts—Geological Association of Canada. Mineralogical Association of Canada Annual Meeting, 11, pp. 127–128.
Sun, S., McDonough, W.R., 1989. Chemical and Isotopic Systematics of Oceanic Basalts: Implications for Mantle Composition and Processes. In: Saunders, A.D., Norry, M.J. (Eds.), 1989, Magmatism in the Ocean Basins. Geological Society Special Publication, 42, pp. 313–345.
Taylor, R.P., 1992. The petrological and geochemical characteristics of the Pleasant Ridge zinnwaldite–topaz granite, southern New Brunswick, and comparisons with other topaz-bearing felsic rocks. The Canadian Mineralogist 30, 895–921.
Taylor, R., 2009. Ore textures—Recognition and Interpretation. Springer-Verlag978-3-642-01782-7 (282 pag.).
Taylor, R.P., Fallick, A.E., 1997. The evolution of fluorine-rich felsic magmas: source dichotomy, magmatic convergence and the origins of topaz granite. Terra Nova 9 (3), 105–108.
Tuttle, O.F., Bowen, N.L., 1958. Origin of granite in the light of experimental studies in the system $NaAlSi_3O_8$–$KAlSi_3O_8$–SiO_2–H_2O. Geological Society of America 74, 153.
Vernon, R.H., 2004. A Practical Guide to Rock Microstructure. Cambridge University Press.
Webster, J.D., 1990. Partitioning of F between H_2O and CO_2 fluids and topaz rhyolite melt Implications for mineralizing magmatic-hydrothermal fluids in F-rich granitic systems. Contributions to Mineralogy and Petrology 104, 424–438.
Whalen, J.B., Currie, K.L., Chappell, B.W., 1987. A-type granites; geochemical characteristics, discrimination and petrogenesis. Contributions to Mineralogy and Petrology 95, 407–419.
Williamson, B.J., Stanley, C.J., Wilkinson, J.J., 1997. Implications from inclusions in topaz for greisenisation and mineralisation in the Hensbarrow topaz granite, Cornwall, England. Contributions to Mineralogy and Petrology 127, 119–128.
Xie, L., Wang, R., Chen, J., Zhu, J., Zhang, W., Lu, J., Zhang, R., 2013. A tin-mineralized topaz rhyolite dike with coeval topaz granite enclaves at Qiguling in the Qitianling tin district, southern China. Lithos 170, 52–268.